ResearchGate

See discussions, stats, and author profiles for this publication at: https://www.researchgate.net/publication/325933516

Investigation of effects of convergence and divergence half-angles on the performance of a nozzle for different operating conditions

Article *in* Journal of the Brazilian Society of Mechanical Sciences and Engineering · July 2018

DOI: 10.1007/s40430-018-1271-9

CITATIONS
2

READS
573

3 authors, including:

Hossein Mahdavy-Moghaddam
Khaje Nasir Toosi University of Technology
5 PUBLICATIONS **6** CITATIONS

SEE PROFILE

Mohamed Jahromi
Dasman Diabetes Institute
43 PUBLICATIONS **629** CITATIONS

SEE PROFILE

Some of the authors of this publication are also working on these related projects:

my phd View project

Kuwaiti Autoimmune Diabetes Study (KADS) View project

All content following this page was uploaded by Hossein Mahdavy-Moghaddam on 05 November 2018.

The user has requested enhancement of the downloaded file.

Journal of the Brazilian Society of Mechanical Sciences and Engineering (2018)40:353
https://doi.org/10.1007/s40430-018-1271-9

TECHNICAL PAPER

Investigation of effects of convergence and divergence half-angles on the performance of a nozzle for different operating conditions

M. H. Hamedi-Estakhrsar[1] · H. Mahdavy-Moghaddam[1] · M. Jahromi[2]

Received: 10 February 2017 / Accepted: 10 June 2018
© The Brazilian Society of Mechanical Sciences and Engineering 2018

Abstract

The effects of convergence and divergence half-angles on the performance of a nozzle at the different pressure ratios are investigated numerically. SST $k-\omega$ turbulence model is applied to simulate the compressible gas flow inside the nozzle and its exhaust plume. Exhaust nozzle performance parameters have been calculated and compared with available experimental data to show the validity of the simulations. For this purpose, different nozzle pressure ratios for various operating conditions including over-expanded, under-expanded and design condition are considered. The effects of the nozzle geometry (convergence and divergence half-angle) on the velocity coefficient (C_v), discharge coefficient (C_d), gross thrust coefficient (C_{fg}) and nozzle adiabatic efficiency (η_n) are investigated. Predicted results show that for a given nozzle pressure ratio, by increasing the divergence angle from 5 to 20, there is about 3% loss in the gross thrust coefficient and also by increasing this angle from 20° to 40°, the value of the C_v and η_n will decrease 5 and 10%, respectively. Increasing the convergence angle reduces the discharge coefficient about 6% and causes a 3% penalty in nozzle gross thrust coefficient.

Keywords Convergence half-angle · Divergence half-angle · Gross thrust coefficient · Discharge coefficient · Velocity coefficient · Nozzle efficiency

List of symbols

A_{throat}	Nozzle throat area (m^2)
A_{eff}	Nozzle effective area (m^2)
C_A	Divergence loss factor
C_d	Discharge coefficient
C_{fg}	Gross thrust coefficient
C_v	Velocity coefficient
C_w	Dimensionless shear stress
F	Thrust (N)
$F_{g-ideal}$	Isentropic thrust (N)
$F_{g-Actual}$	Actual thrust (N)
G_k	Production of k
G_ω	Production of ω
k	Turbulent kinetic energy (m^2/s^2)
L	Length of nozzle (m)
$\dot{m}$	Actual mass flow rate (kg/s)
$\dot{m}_{ideal}$	Isentropic mass flow rate (kg/s)
NPR	Nozzle pressure ratio ($P_{inlet}/P_{ambient}$)
P_a	Ambient pressure (Pa)
P_0	Back pressure (Pa)
P_e	Exit pressure (Pa)
P_{ti}	Inlet stagnation pressure (Pa)
P_{tt}	Throat stagnation pressure (Pa)
P_{te}	Exit stagnation pressure (Pa)
R	Gas constant (kj/kg K)
S_k	User-defined source term
S_ω	User-defined source term
T_t	Stagnation temperature (K)
$V_{e-ideal}$	Isentropic exit velocity (m/s)
V_e	Exit velocity (m/s)
$\bar{u}$	Average gas velocity (m/s)
u'	Fluctuating velocity component (m/s)
β	Divergence half-angle (degree)
Y_k	Dissipation of k
Y_ω	Dissipation of ω
Γ_k	Diffusion coefficient of k
Γ_ω	Diffusion coefficient of ω

Technical Editor: Jader Barbosa Jr.

✉ H. Mahdavy-Moghaddam
mahdavy@kntu.ac.ir

[1] Faculty of Aerospace Engineering, K. N. Toosi University of Technology, Tehran, Iran

[2] Faculty of Aerospace Engineering, Malek-Ashtar University of Technology, Tehran, Iran

Published online: 22 June 2018

γ	Specific heat ratio
η_n	Nozzle efficiency (%)
θ	Convergence half-angle (degree)
μ	Dynamic viscosity(Pa s)
μ_t	Turbulent dynamic viscosity (Pa s)
ρ	Flow field density (kg/m^3)
σ_k	Turbulent Prandtl numbers for k
σ_ω	Turbulent Prandtl numbers for ω
τ_w	Wall shear stress

1 Introduction

The exhaust nozzle is a very important component of the overall engine propulsion systems. The converging–diverging nozzles are used to accelerate the fluid to supersonic speeds past the throat of such a nozzle. In this case, depending on the ratio of the average outlet pressure to the inlet stagnation pressure, there is a possibility of creating shock waves in the flow field [1]. It is highly important to be able to predict the thrust efficiency for a given nozzle geometry. The efficiency of an engine exhaust nozzle, usually represented by the gross thrust coefficient (C_{fg}), is defined as the ratio of the actual nozzle gross thrust to the ideal gross thrust.

Nozzle performance was considered in many experimental and numerical studies, especially from the point of flow and heat transfer characteristics with various inlet boundary conditions and flow geometries. Mason et al. [2] conducted an experiment to determine the effect of throat contouring on the nozzle internal performance. They tested five non-axisymmetric converging–diverging nozzles in the static test facility of the Langley 16-foot transonic tunnel and recorded internal performance data at different nozzle pressure ratios up to 9.0.

Park et al. [3] investigated sonic nozzles that are applied to gas flow rate measurements and determined that the critical pressure ratio is highly dependent on the Reynolds number rather than area ratio, especially in the cases with low flow velocity. Variation of discharge coefficients for sonic nozzles with flow geometry and Reynolds number was reported by Paik et al. [4], who determined higher discharge coefficients with increase of mass flow rate. Spotts et al. [5] performed a CFD study of the compressible flow through convergent–conical nozzles to investigate the effect of the nozzle pressure ratio and nozzle angle on the nozzle performance. They confirmed that for smaller nozzle angles, the discharge coefficient increases and the choked nozzle pressure ratio will be reduced.

Geatz [6] developed a computational code for prediction of the thrust performance characteristics of non-axisymmetric two-dimensional convergent–divergent exhaust nozzles. The code includes the effects of friction, angularity and expansion losses on the overall nozzle efficiency. To demonstrate the validity of code, the predicted results were compared with experimental data for a number of different nozzle geometries. The code showed excellent agreement with experimental data in predicting the peak gross thrust coefficients for basic 2D-CD nozzle geometries.

Although there is a large amount of studies concerning the flow through the CD nozzles over a wide range of nozzle pressure ratios (NPRs), the detailed investigation on the effects of the both convergence and divergence half-angle for the constant expansion ratio (A_e/A_t) on the gross thrust coefficient, the velocity coefficient, the discharge coefficient and the adiabatic efficiency in CD nozzle is less studied. In this paper, the supersonic flow inside a 2D converging–diverging nozzle and its exhaust plume are simulated numerically with SST $k-w$ turbulence model and the results are compared to the experimental data of Mason et al. [2]. Then, the parametric study is carried out in which the convergence half-angle, divergence half-angle and nozzle pressure ratio (NPR) are variable. Attention is paid to the effect of nozzle angle on nozzle performance and changes in the value of the gross thrust coefficient (C_{fg}), the velocity coefficient (C_v), discharge coefficient (C_d) and the nozzle adiabatic efficiency (η_n).

2 Selection of the turbulence model

Selection of a suitable turbulence model for proper prediction of the turbulent flow is an important part of a good simulation. Hamed and Vogiatzis [7] assessed several turbulence models in terms of their effects on the agreement between the experimental centerline pressure distribution and the 2D computational results at over-expanded conditions. Their results indicated that both the prediction of the shock location and pressure level behind the shock strongly depends on the applied turbulence model. Many authors reported that the standard $k-\varepsilon$ model fails to predict the mean velocity profiles of turbulent axisymmetric jets accurately (see, e.g., Thies and Tam [8]). Chenault and Beran [9] conducted a numerical investigation of supersonic injection using second-order Reynolds-stress turbulence model proposed by Zhang et al. [10] as well as the $k-\varepsilon$ model. Detailed comparison with experimental data showed that the Reynolds-stress model simulation results are physically consistent and accurate prediction for jet plume mean flow and turbulent quantities. On the other

hand, the simulations with the $k-\varepsilon$ model resulted in nonphysical and inconsistent turbulence prediction.

The accuracy of turbulent jet plume prediction significantly depends on the numerical method and turbulence model. Dembowski and Georgiadis [11] conducted a numerical study for supersonic axisymmetric jet flow using two-equation SST and $k-\varepsilon$ model with and without compressibility correction. Their results indicated that these models do not predict supersonic nozzle flows accurately.

Xiao et al. [12] investigated the compressible jet plume from a planar over-expanded nozzle by solving the Reynolds-averaged Navier–Stokes (RANS) equations with several turbulence models. By comparing the simulation results with available experimental data, they showed that two-equation shear stress model (SST) gives the best results and the simulations are able to predict the velocity profiles, total pressure decay and axial jet thickness distribution in the jet plume reasonably well.

Balabel et al. [13] applied the turbulent gas flow dynamics in a two-dimensional convergent–divergent rocket nozzle and predicted the associated physical phenomena for various operating conditions. Different turbulence models are applied and assessed by comparing the obtained results of the static wall pressure and the shock position with the available experimental data. The dimensionless shear stress at the nozzle wall and the separation point are also predicted. Among the turbulence models adopted, the shear stress transport (SST) $k-\omega$ model gave the best overall agreement with the experimental measurements.

Recently, compressible flow passing through a 2D convergent–divergent nozzle with a fixed geometry and different nozzle pressure ratios is simulated by Balabel et al. [14] with several turbulence models, namely the standard $k-\varepsilon$ model, the extended $k-\varepsilon$ model, shear-stress transport $k-\omega$ model, Reynolds stress model, $v^{2}-f$ model and the realizable $v^{2}-f$ model. The numerical results reveal that the SST $k-\omega$ and the realizable $v^{2}-f$ models give the best results compared with other models in predicting the shock wave position and the separation point, while other models give a poor prediction.

According to above, it seems that the SST $k-\omega$ turbulence model showed the better predictions than the other turbulence models. Therefore, in this study, the SST $k-\omega$ turbulence model is used to investigate the effect of nozzle convergence half-angles and divergence half-angles on the turbulent flow behavior inside the convergent–divergent nozzle and its exhaust plume.

3 Problem definition

In this paper, the geometry of CD nozzle which was studied by Mason et al. [2] is used as baseline nozzle geometry. The schematic of nozzle geometry is shown in Fig. 1. The design parameters for the configuration of the baseline nozzle geometry are provided in Table 1 as well.

This baseline geometry was modified by changing the convergence half-angle (θ) from 20.84° to 5°, 10°, 30° and 40° and divergence half-angle (β) from 10.85° to 5°, 20°, 30° and 40° while the parameters h_e (exit area) and h_i (throat area) are kept constant.

For a parametric study, the nozzle pressure ratio (NPR) has been changed in the range of 1–20. All special conditions of the nozzle performance, i.e., under-expanded, over-expanded, fully expanded and creation of the normal shock are considered in the simulations.

The expansion ratio (ratio of exit area to throat area) of the baseline CD nozzle is 1.8, so by using the gas dynamics relations, the value of nozzle pressure ratio will be 8.81.

4 Governing equation

The FLUENT software is used to solve the Reynolds-averaged Navier–Stokes (RANS) equation with turbulence models. The governing equations, which include the conservation equations for mass, momentum and energy, along with the equation of state, are written in generalized coordinates and in conservative form. The continuity and momentum equations can be written in Cartesian tensor form as:

$$\frac{\partial \rho}{\partial t}+\frac{\partial}{\partial x_i}(\rho u_i)=0 \tag{1}$$

$$\frac{\partial}{\partial t}(\rho u_i)+\frac{\partial}{\partial x_j}(\rho u_i u_j)=-\frac{\partial p}{\partial x_i}+\frac{\partial}{\partial x_j}\left[\mu\left(\frac{\partial u_i}{\partial x_j}+\frac{\partial u_j}{\partial x_i}-\frac{2}{3}\delta_{ij}\frac{\partial u_i}{\partial x_i}\right)\right]+\frac{\partial}{\partial x_j}\left(-\rho\overline{u_i' u_j'}\right) \tag{2}$$

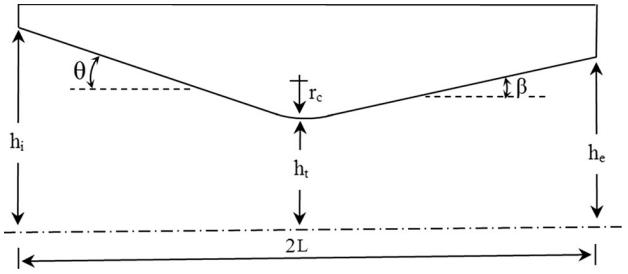

Fig. 1 Schematic of nozzle geometry

Table 1 Design parameters of baseline nozzle geometry (all dimensions are in cm)

Parameter	θ	β	r_c	h_e	h_t	h_i	A_e/A_t
Value	20.84	10.85	0.68	2.46	1.37	3.52	1.8

Equations (1) and (2) are called Reynolds-averaged Navier–Stokes (RANS) equations.

They have the same general form as the instantaneous Navier–Stokes equations, with the velocities and other solution variables now representing time-averaged values. Additional terms now appear that represent the effects of turbulence. These Reynolds stresses $\left(-\rho\overline{u_i'u_j'}\right)$ must be modeled in order to close Eq. (2) [15].

Turbulence modeling was required to predict solutions for the flow field of this study. FLUENT has several turbulence simulations by implementing either a two-equation, linear or nonlinear model [16].

The shear stress transport (SST) $k-\omega$ model is employed to predict the flow behavior in the considered physical domain. The shear stress transport (SST) $k-\omega$ model was developed by Menter [17] to effectively blend the robust and accurate formulation of the $k-\omega$ model in the near-wall region with the free-stream independence of the $k-\varepsilon$ model in the far field. In this model, the definition of the turbulent viscosity is modified to account for the transport of the turbulent shear stress.

Transport equations for k and ω in SST model are as follows:

$$\frac{\partial}{\partial t}(\rho k)+\frac{\partial}{\partial x_i}(\rho k u_i)=\frac{\partial}{\partial x_j}\left(\Gamma_k\frac{\partial k}{\partial x_j}\right)+G_k-\Upsilon_k+S_k \tag{3}$$

And

$$\frac{\partial}{\partial t}(\rho\omega)+\frac{\partial}{\partial x_i}(\rho\omega u_i)=\frac{\partial}{\partial x_j}\left(\Gamma_\omega\frac{\partial\omega}{\partial x_j}\right)+G_\omega-\Upsilon_\omega+S_\omega \tag{4}$$

The term G_k represents the production of turbulence kinetic energy due to mean velocity gradient that can be calculated by

$$G_k=-\rho\overline{u_i'u_j'}\frac{\partial u_j}{\partial x_i} \tag{5}$$

The production of ω is shown by equation

$$G_\omega=\alpha\frac{\omega}{k}G_k \tag{6}$$

The coefficient α is a function of k and ω and it is so calculated that in the far field regions of flow approaches to unity.

Where Γ_k and Γ_ω represent the effective diffusivity of k and ω, respectively, that is defined as

$$\Gamma_k=\mu+\frac{\mu_t}{\sigma_k} \tag{7}$$

And

$$\Gamma_\omega=\mu+\frac{\mu_t}{\sigma_\omega} \tag{8}$$

where σ_k and σ_ω are the turbulent Prandtl numbers for k and ω, respectively. μ_t is the turbulent viscosity, Υ_k and Υ_ω represent the dissipation of k and ω due to turbulence. S_k and S_ω are user-defined source terms [15].

5 Exhaust nozzle performance parameter

The nozzle contribution to engine thrust is called gross thrust. It comprises two terms, namely the momentum thrust and the pressure thrust.

$$F=\dot{m}V_e+(P_e-P_0)A_e \tag{9}$$

Nozzle total pressure ratio (π_n) has been identified as

$$\pi_n=\frac{P_{te}}{P_{ti}} \tag{10}$$

This parameter is a direct measure of flow irreversibility, that is, due to friction and shock, in the nozzle. An important operational parameter of a nozzle is the NPR. It is defined as

$$\mathrm{NPR}=\frac{P_{ti}}{P_0} \tag{11}$$

This parameter, that is, the nozzle pressure ratio, signifies the nozzle flow expansion potential (i.e., from the stagnation or total state at the exit to the ambient static state).

For an ideal gas, in an adiabatic nozzle flow, η_n, π_n, NPR are related to each other, via

$$\eta_n=\frac{\left\{\mathrm{NPR}\left(\frac{P_0}{P_e}\right)\right\}^{\frac{\gamma-1}{\gamma}}-\pi_n^{-\frac{\gamma-1}{\gamma}}}{\left\{\mathrm{NPR}\left(\frac{P_0}{P_e}\right)\right\}^{\frac{\gamma-1}{\gamma}}-1} \tag{12}$$

The combined effect of these parameters on the mass flow rate is represented through a discharge coefficient C_D as

$$C_D=\frac{\dot{m}}{\dot{m}_{ideal}} \tag{13}$$

where the numerator is the actual mass flow rate through the nozzle throat and denominator is the ideal mass flow rate based on the geometrical throat area. The subscript, "ideal," refers to quantities calculated for an ideal nozzle

based on one-dimensional isentropic flow assumption. The isentropic mass flow rate ($\dot{m}_{\text{ideal}}$) is calculated by [6]

$$\dot{m}_{\text{ideal}} = \frac{P_t A_{\text{throat}}}{\sqrt{RT_t}} \sqrt{\gamma} \left(\frac{2}{\gamma + 1} \right)^{\frac{\gamma+1}{2(\gamma-1)}}, \tag{14}$$

where γ is the specific heat ratio (γ = 1.4), R is the gas constant (R = 287 J/kg K), P_t and T_t are stagnation conditions.

The nozzle thrust coefficient and the discharge coefficient for all the cases in the parametric study have been calculated using the above relations.

A velocity coefficient (C_v) that measures the extent of viscous flow losses in the exhaust is defined by

$$C_V = \frac{V_e}{V_{\text{eideal}}}, \tag{15}$$

where the numerator is the actual exhaust velocity and the denominator is the ideal exhaust velocity with no loss of total pressure $P_{te} = P_{tt}$. Therefore, $V_{e\ \text{ideal}}$ is the ideal exit velocity only if the divergent section of the nozzle were isentropic [18].

After some manipulation, we may show the following expression for the velocity coefficient:

$$C_V = \sqrt{\frac{\left[1 - \left(\frac{P_e/P_0}{\text{NPR} \cdot \pi_n} \right)^{\frac{\gamma-1}{\gamma}} \right]}{\left[1 - \left(\frac{P_e/P_0}{\text{NPR} \cdot C_D^2} \right)^{\frac{\gamma-1}{\gamma}} \right]}} \tag{16}$$

For a two-dimensional convergent–divergent nozzle, we can derive the angularity loss factor or divergence loss factor (C_A), in a straightforward manner, using the definition as

$$C_A = \frac{\sin(\beta)}{\beta}, \tag{17}$$

where β is the divergence half-angle of the nozzle. Note that the β in the denominator of C_A must be in radians (not degrees).

We define a nozzle gross thrust coefficient C_{fg} according to

$$C_{fg} = \frac{F_{g-\text{actual}}}{F_{g-\text{ideal}}} \tag{18}$$

Hence, the gross thrust coefficient becomes

$$C_{fg} = C_D C_V \sqrt{\frac{1 - \left(\frac{P_e/P_0}{\text{NPR} \cdot C_D^2} \right)^{\frac{\gamma-1}{\gamma}}}{1 - \text{NPR}^{-\frac{\gamma-1}{\gamma}}}} \left[C_A + \frac{\frac{\gamma-1}{2\gamma} \left(1 - \frac{P_0}{P_e} \right)}{\left(\pi_n \text{NPR} \frac{P_0}{P_e} \right)^{\frac{\gamma-1}{\gamma}} - 1} \right] \tag{19}$$

The momentum thrust is affected by total pressure losses and flow angularity at the exit, which is the first term of the bracket [18].

6 Boundary conditions

Boundary conditions are specified for the inlet, outlets and solid nozzle walls. The boundary condition of pressure inlet at the entrance to the nozzle is considered. The primary nozzle flow is implemented with a total temperature (300 K) and total pressure that are obtained from the design nozzle pressure ratio (NPR_d = 8.81). At the outlet, the boundary condition of pressure far field with very small Mach number of 0.01 is performed for the ambient region to avoid the solution divergence due to large gradient [16].

The simulation is two-dimensional, and all of the walls are considered no heat flux. At walls, no-slip boundary conditions were imposed on the gas velocity components. Symmetry boundary condition is applied at the nozzle centerline. A 2D computational domain with the assigned boundary conditions is shown in Fig. 2.

7 Grid generation and results verification

Three different grids were generated to simulate the gas flow inside the baseline geometry of CD nozzle and its exhaust plume.

Figure 3 shows the predicted pressure distribution on the nozzle sidewall using three different grids at design nozzle pressure ratio of 8.81. The static wall pressure is normalized using the total pressure (P_t) and plotted against the dimensionless axial location x/L, where L is the length of the nozzle. The results are presented for a coarse mesh (50 × 150), a medium mesh (100 × 200) and a fine mesh (150 × 250) inside the CD nozzle. A total number of cells inside and outside the nozzle are 23,000, 36,000 and 56,000 cells for the coarse mesh (Grid A), the medium mesh (Grid B) and the fine mesh (Grid C), respectively.

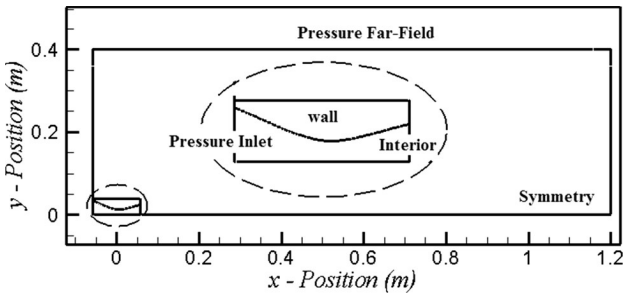

Fig. 2 Two-dimensional computational domain with the assigned boundary conditions

The comparison shows that the results obtained using Grid B and Grid C inside the CD nozzle are very close. Therefore, the simulations were performed on Grid B (36,000 quadrilateral cells) to reduce the computational time.

Figure 4a shows the medium mesh (Grid B). Details of the mesh near the nozzle are also shown in Fig. 4b.

8 Validation of results

Numerical solutions of the supersonic gas flow inside the converging–diverging nozzle have been performed using FLUENT Software.

Airflows with the viscosity of $\mu = 1.789 \times 10^{-5}$ Ns/m^2 are simulated. The nozzle pressure ratios in the range of 6–10 are considered in the simulations. The compressible, steady-state, Reynolds-averaged Navier–Stokes equations were solved using a density-based method. The governing equations are discretized using the finite-volume method with the second-order upwind.

The residual of 10^{-4} is selected as the convergence criterion for termination of the solution procedure of the equations.

In Fig. 5, the predicted gross thrust coefficient is compared with the experimental data of Mason et al. [2] for the baseline geometry. The results are in good agreement with the experimental data for the NPRs in the range of 6–10. It is seen that the maximum overprediction of the numerical simulations is 1%.

Predicted discharge coefficient is compared with the experimental data of Mason et al. [2] in Fig. 6. The accuracy of the predicted results shows the reliability of the simulation method.

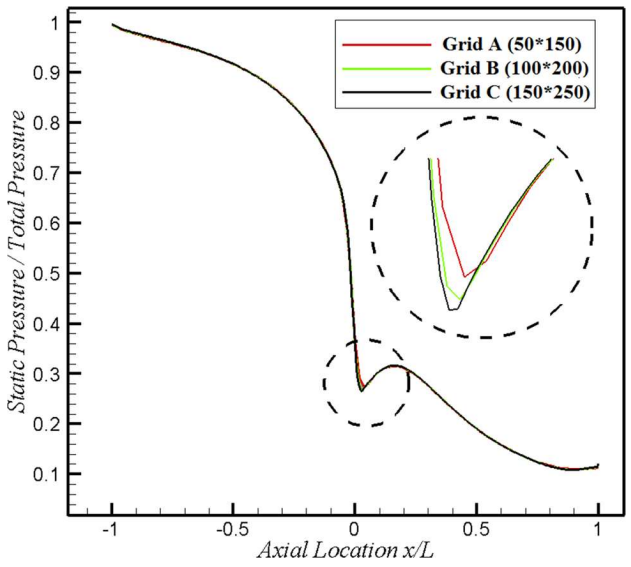

Fig. 3 Comparison of predicted pressure distribution on the nozzle sidewall for different grids

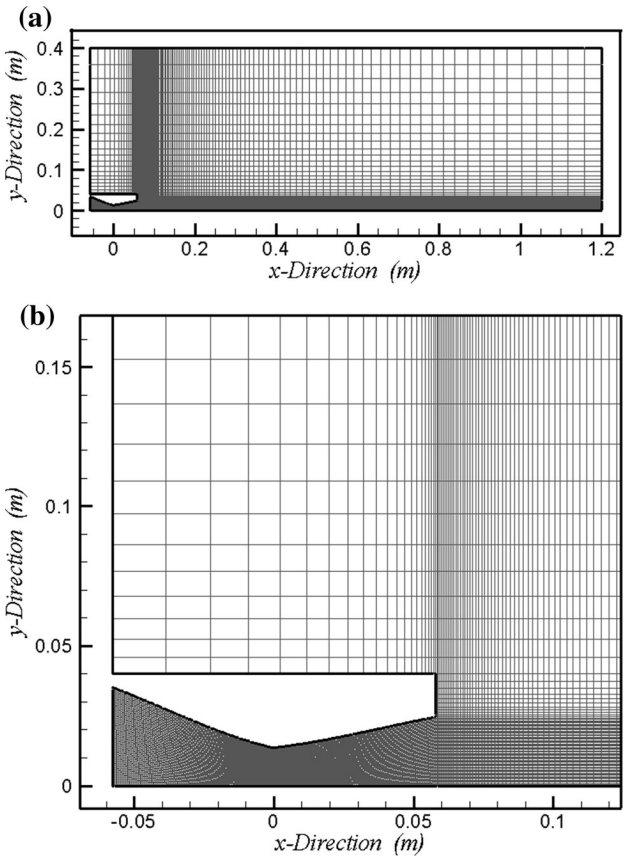

Fig. 4 Mesh generated for gas flow computation: **a** whole of the domain and **b** details of mesh near the nozzle

9 Result and discussion

9.1 Effect of nozzle pressure ratio (NPR)

Contours of computed Mach number for different NPRs (17.62, 8.81, 4.41, 2.94 and 1.82) are plotted in Fig. 7 for baseline geometry ($\beta = 10.85°$, and $\theta = 20.84°$). The results are obtained for different ambient pressures. Different values of $P_0 = 0.5$ atm (under-expansion), 1 atm. (full-expansion), 2 atm. (over-expansion), 3 and 4.8 atm. (normal shock inside of the divergent section and at the outlet area of the nozzle) are considered in the simulations.

These contours describe the influence of the nozzle pressure ratio on the gas flow characteristics inside the nozzle and its exhaust plume. For more discussion, variations of the pressure on the upper wall of the nozzle are shown in Fig. 8. As shown, by increasing the NPR or decreasing the back pressure, the position of the normal shock moves from the throat to the exit area of the nozzle.

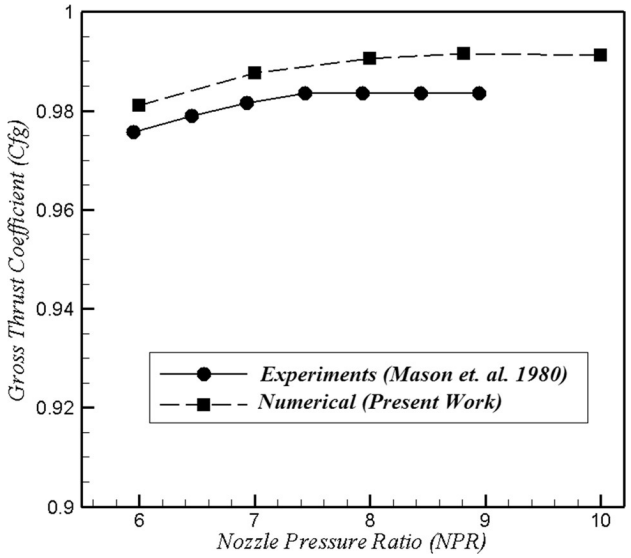

Fig. 5 Comparison of the gross thrust coefficient prediction results to the experimental data

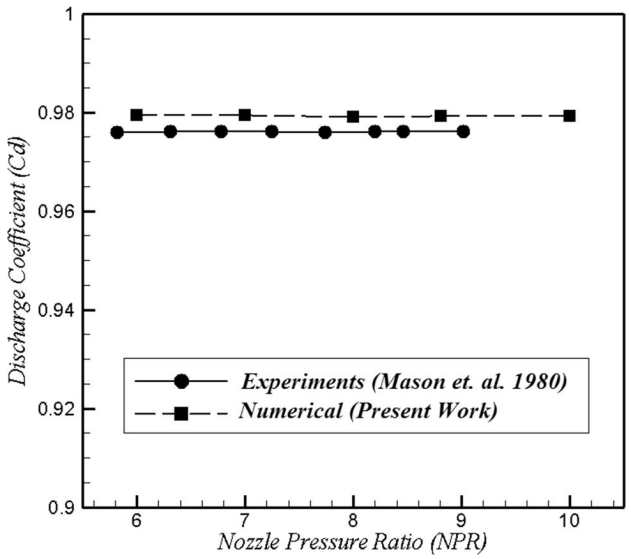

Fig. 6 Comparison of the discharge coefficient prediction results to the experimental data

The skin friction coefficient

$$\left(C_w = \frac{\tau_w}{1/2\rho v^2}\right)$$

distribution for different NPRs is plotted in Fig. 9, where v is the gas velocity at the nozzle inlet. For flows at low NPRs, the results indicate that the flow did not reattach to the nozzle wall and cause separation. By decreasing the ambient pressure, separation occurs near the exit plane of the nozzle. On the other hand, by decreasing the NPR, the separation point occurs near the nozzle throat.

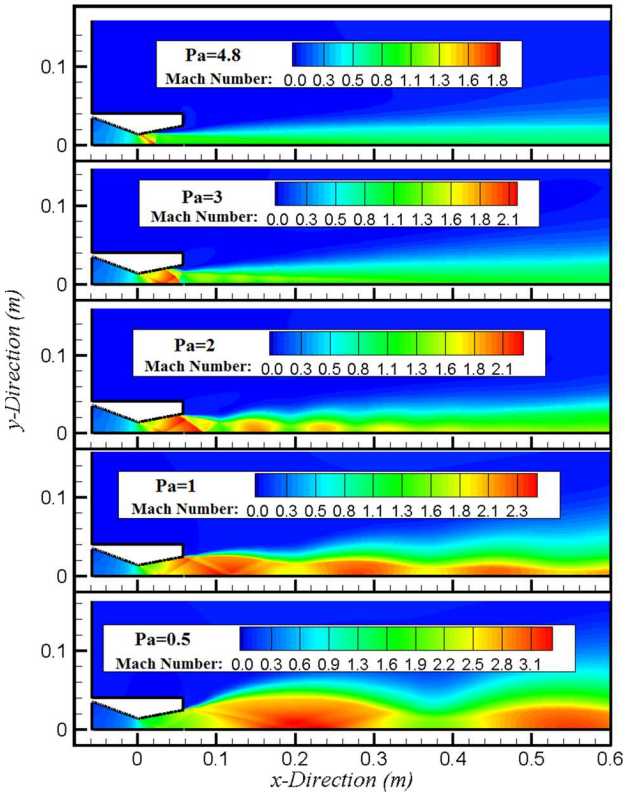

Fig. 7 Illustration of the computed Mach number contours for different back pressures

9.2 Effect of divergence half-angle (β)

In this section, various divergence half-angles of CD nozzle (β = 5°, 10.85°, 20°, 30 and 40°) have been considered in simulations. The convergence half-angle (θ = 20.84°) is

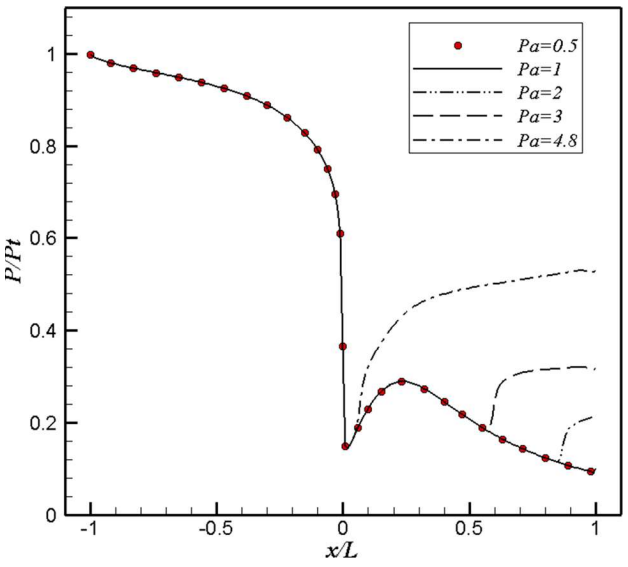

Fig. 8 Comparison of normalized pressure distributions along the nozzle sidewall for different back pressures

kept constant. The contours of Mach number for the mentioned cases at nozzle pressure ratio of 8.81 are shown in Fig. 10. The CD nozzle with (β = 10.85°) is the baseline geometry which was studied by Mason et al. [2] and Krishnamurty et al. [19] (see Fig. 10). As shown, the divergence half- angle has a great effect on the nozzle performance, the location of the shock, the type of shock wave and the number of shock.

Variations of the discharge coefficient for different geometries are shown in Fig. 11. As expected, C_d is almost independent of nozzle pressure ratio since the nozzles were choked for all cases in the numerical simulations. Also, the divergence half-angle has no significant effect on the discharge coefficient (about 1%).

The predicted velocity coefficients and nozzle efficiencies for various divergence half-angles (β) are shown in Figs. 12 and 13, respectively. These figures show that increasing the divergence angle reduces the velocity coefficient and the adiabatic efficiency of the nozzle in such a way that, at the design nozzle pressure ratio (NPR = 8.81), by increasing the value of β from 20° to 40°, the values of C_v and η_n will decrease by 5 and 10%, respectively. The decrease in the predicted values of C_v and η_n for the nozzle with β = 10 at NPR of 2.94 is the creation of normal shock at the exit area of the nozzle.

In Fig. 14, the gross thrust coefficients for the nozzles with various divergence angles are plotted against the nozzle pressure ratio. Variations of the gross thrust coefficient for all NPRs have the same behavior. For each configuration, C_{fg} increases from a minimum value at the lowest nozzle pressure ratio to a peak level near the design nozzle pressure ratio of 8.81.

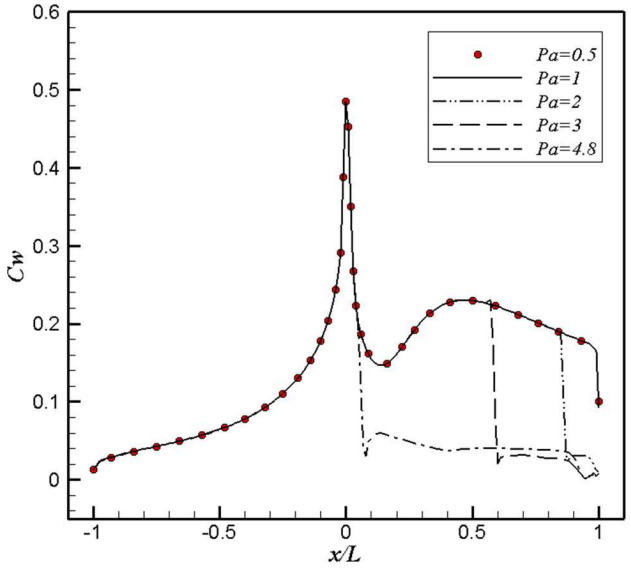

Fig. 9 Comparison of dimensionless wall shear stress distributions along the nozzle sidewall for different back pressures

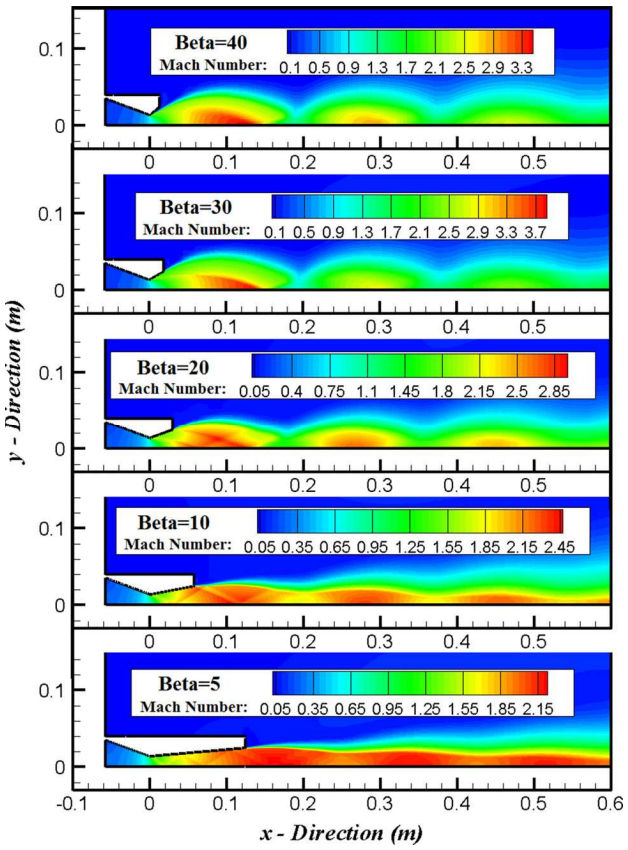

Fig. 10 Contour of Mach number and geometries of CD nozzle with various divergence half-angles (β = 5°, 10.85°, 20°, 30 and 40°) at design nozzle pressure ratio of 8.81

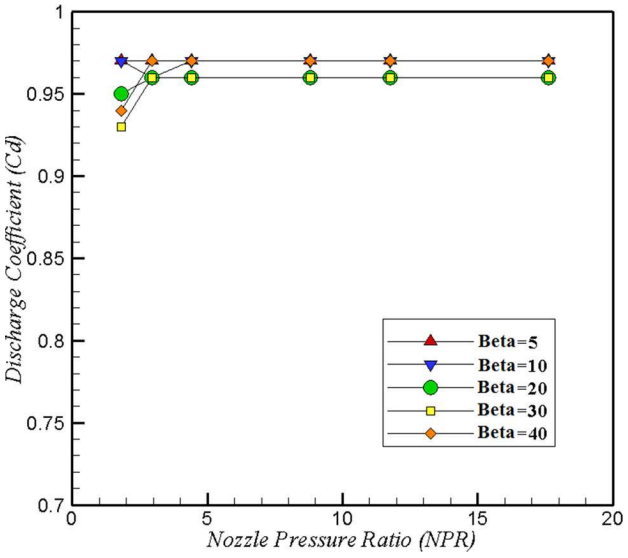

Fig. 11 Discharge coefficient (C_d) for the nozzles with various divergence angles (β) into the nozzle pressure ratio

This figure shows that for a given nozzle pressure ratio, the gross thrust coefficient is higher for smaller divergence angles. By increasing the divergence angle (β) from 5 to

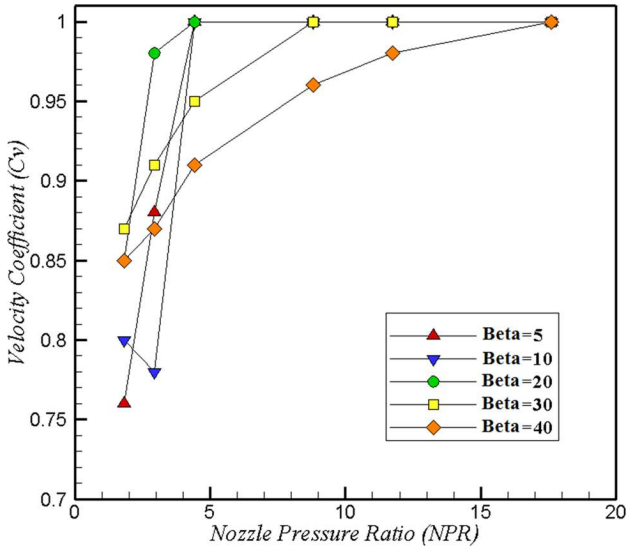

Fig. 12 Velocity coefficient (C_v) for the nozzles with various divergence angles (β) into the nozzle pressure ratio

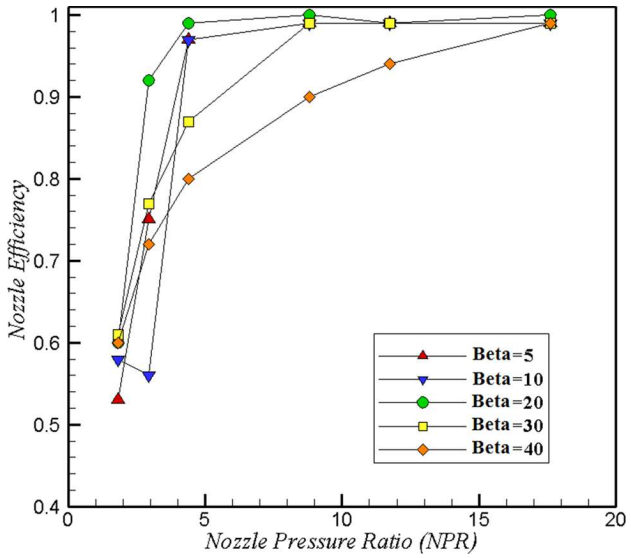

Fig. 13 Nozzle efficiency (η_n) for the nozzles with various divergence angles (β) into the nozzle pressure ratio

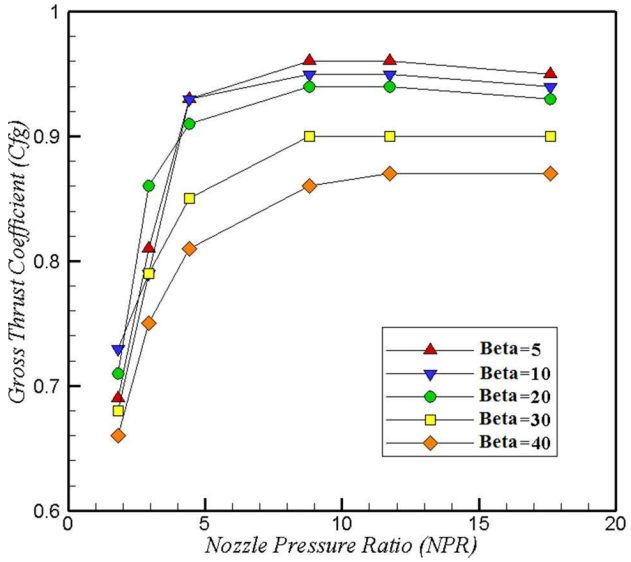

Fig. 14 Gross thrust coefficient (C_{fg}) for the nozzles with various divergence angles (β) into the nozzle pressure ratio

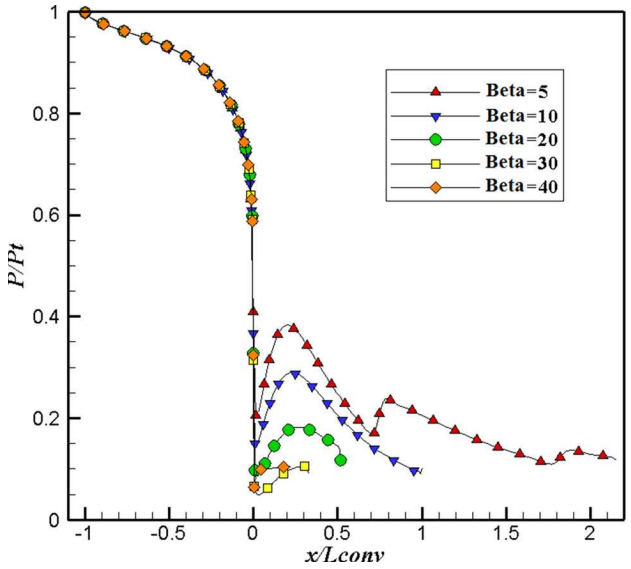

Fig. 15 Comparison of normalized pressure distributions along the nozzle sidewall for the nozzles with various divergence angles

20, there is about 3% change in the gross thrust coefficient. More increment in β from 20° to 40° leads to about 9% decrease in C_{fg}.

Variations of the static pressure on the upper wall of the nozzle are presented in Fig. 15 for nozzle pressure ratio of NPR = 8.81. In this Figure, the local static pressure is normalized by the inlet total pressure (P_t), and the x coordinate is normalized by the length of the convergent part of the nozzle.

The predicted results of skin friction coefficient (C_w) on the upper wall of the nozzle are shown in Fig. 16. The results were presented for the pressure ratio of 8.81. As can be seen, for a large divergence angles (β = 40°), the separation phenomena (C_w = 0) will occur near the nozzle throat area. From the results of these figures (Figs. 15, 16) it can be concluded that the location of the shock in the nozzle and the separation point are affected by the NPR and divergence half-angle.

9.3 Effect of convergence half-angle (θ)

Nozzles with different convergence half-angles (θ = 5°, 10°, 20.84°, 30° and 40°) and constant divergence half-angle of β = 10.85° have been investigated numerically.

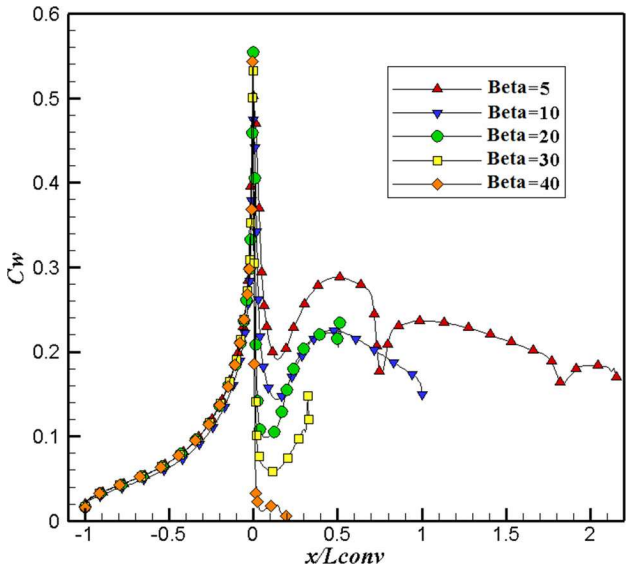

Fig. 16 Comparison of dimensionless wall shear stress distributions along the nozzle sidewall for the nozzles with various divergence angles

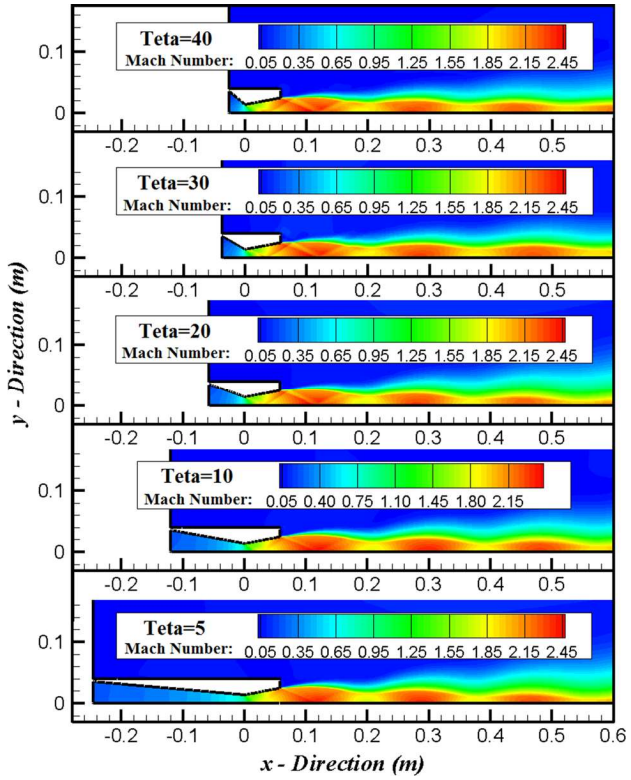

Fig. 17 Contour of Mach number and geometries of CD nozzle with various convergence half-angles (θ = 5°, 10°, 20.84°, 30 and 40°) at design nozzle pressure ratio of 8.81

Contours of Mach number inside and outside of the CD nozzle are shown in Fig. 17, at design nozzle pressure ratio of 8.81. As shown, the change in the convergence half-angle has no significant effect on the pattern of the exhaust plume.

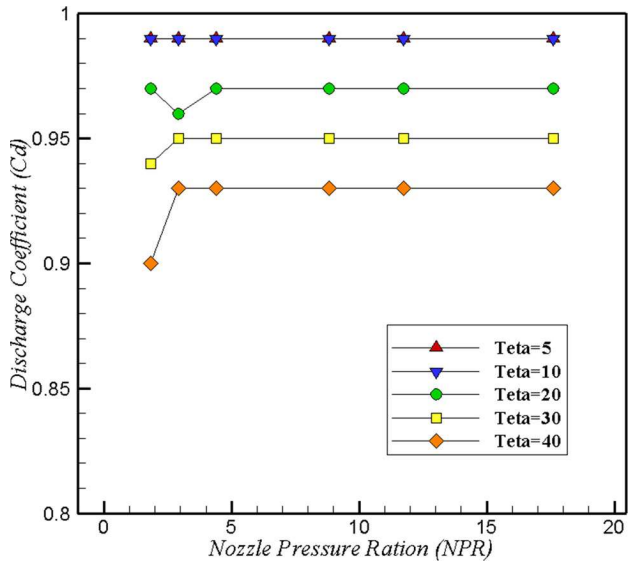

Fig. 18 Discharge coefficient (C_d) for the nozzles with various convergence angles (θ) into the nozzle pressure ratio

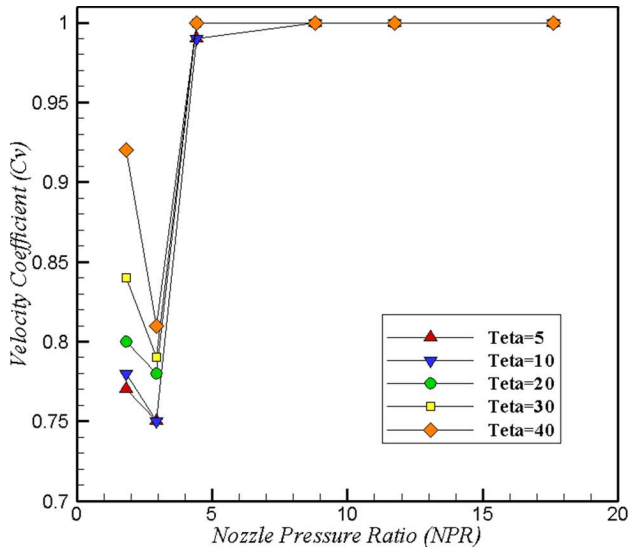

Fig. 19 Velocity coefficient (C_v) for the nozzles with various convergence angles (θ) into the nozzle pressure ratio

Variations of discharge coefficient with the nozzle pressure ratio at different convergence angles are shown in Fig. 18. It can be seen that for larger values of θ, the discharge coefficient will decrease 6%. Note that the result of the C_d is almost independent of nozzle pressure ratio because the gas flow in the nozzles was choked.

By changing the convergence angle from 5° to 40°, there has been no change (about 1%) in the value of the nozzle adiabatic efficiency and the velocity coefficient for NPRs 5–20 (see Figs. 19, 20). As mentioned, the reduction in

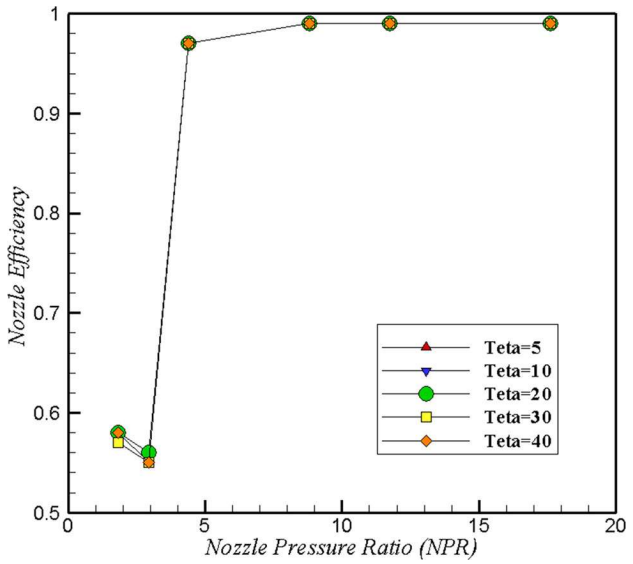

Fig. 20 Nozzle efficiency (η_n) for the nozzles with various convergence angles (θ) into the nozzle pressure ratio

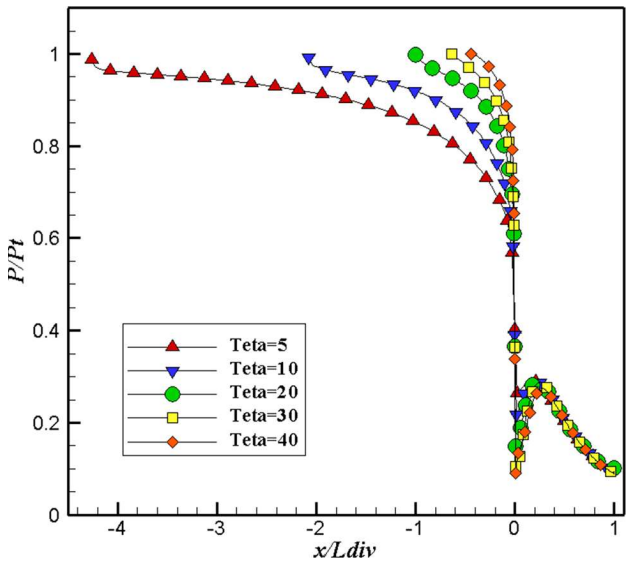

Fig. 22 Comparison of normalized pressure distributions along the nozzle sidewall for the nozzles with various convergence angles

predicted value of the C_v and η_n in the nozzle with $\beta = 10°$ and NPR = 2.94 is the creation of a normal shock at the exit area of the nozzle.

Effects of the nozzle pressure ratio on the gross thrust coefficient (C_{fg}) are illustrated in Fig. 21. The results were presented for different convergence angles. As shown, the shapes of the curves are identical and all curves have a maximum value at the design pressure ratio of 8.81.

At large pressure ratios, each 10° increment in the convergence angle causes about 3% reduction in the thrust coefficient. Increasing the convergence angle had a negative impact on gross thrust coefficient and discharge coefficient.

Finally, variations of the pressure distribution and skin friction coefficient on the upper wall of the nozzle at different convergence half-angles are illustrated in Figs. 22 and 23. These figures show that by increasing the convergence angle, separation occurs near the nozzle throat. For this reason, at the convergence angle of 40°, the wall shear stress after the throat falls to zero and separation occurs.

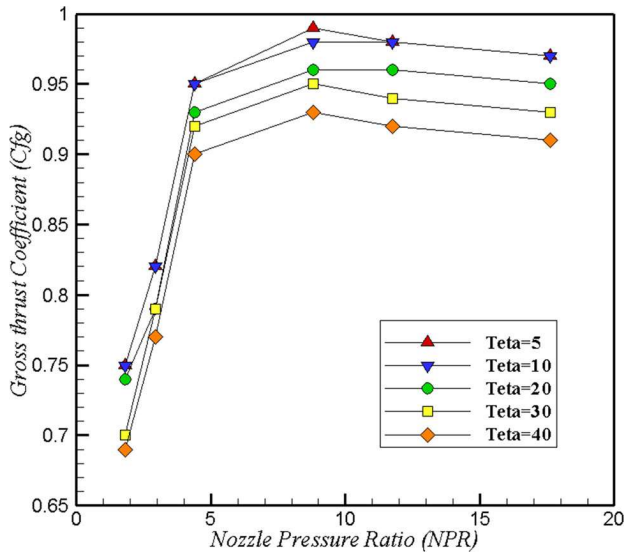

Fig. 21 Gross thrust coefficient (C_{fg}) for the nozzles with various convergence angles (θ) into the nozzle pressure ratio

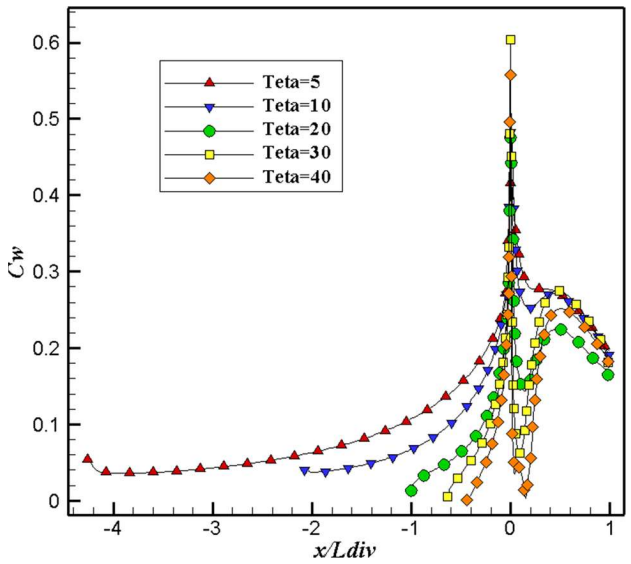

Fig. 23 Comparison of dimensionless wall shear stress distributions along the nozzle sidewall for the nozzles with various convergence angles

10 Conclusions

Compressible gas flow inside a converging–diverging nozzle at different pressure ratios has been numerically studied by SST $k-\omega$ turbulence model. Effects of the changes in convergence half-angle (θ) and divergence half-angle (β) on the nozzle performance, including discharge coefficient (C_d), velocity coefficient (C_v), nozzle efficiency (η_n) and gross thrust coefficient (C_{fg}), have been numerically investigated. For validation of the numerical method, the predicted results of C_{fg} and C_d were compared with available experimental data of Mason et al. [2].

Some important findings of this study can be summarized as:

- Divergence half-angle has no significant effects (about 1%) on the discharge coefficient.
- At the design nozzle pressure ratio (NPR = 8.81) by increasing the divergence half-angle from 20° to 40°, the value of the C_v and η_n will decrease 5 and 10%, respectively.
- By increasing the divergence angle from 5 to 20, there is about 3% loss in the gross thrust coefficient. More increment in β from 20 to 40° leads to about 9% decrease in C_{fg}.
- The discharge coefficient will decrease 6% by increasing the convergence angles from 5° to 40°.
- Each 10° increment in convergence angle in the range of 10°–40° caused a 3% penalty in nozzle gross thrust coefficient.
- At convergence angle of 40°, the wall shear stress after the nozzle throat falls to zero and separation occurs.

References

1. Quintao KK (2012) Design optimization of nozzle shapes for maximum uniformity of exit flow. M.S. Thesis, Florida International University
2. Mason ML, Putnam LE, Richard JR (1980) The effect of throat contouring on two dimensional converging-diverging nozzles at static condition. NASA technical paper 1704
3. Park KA, Choi YM, Choi HM, Cha TS, Yoon BH (2001) The evaluation of critical pressure ratios of sonic nozzles at low Reynolds numbers. Flow Meas Instrum 12:37–41
4. Paik JS, Park KA, Park JT (2000) Inter-laboratory comparison of sonic nozzles at KRISS. Flow Meas Instrum 11:339–344
5. Spotts N, Guzik S, Gaoz X (2007) A CFD analysis of compressible flow through convergent-conical nozzles. AIAA, New York
6. Geatz AM (2005) A prediction code for the thrust performance of two dimensional, non-axisymmetric, converging diverging nozzles. Ph.D. thesis, Air Force Institute of Technology
7. Hamed A, Vogiatzis C (1996) Assessment of turbulence models in over-expanded 2DCD nozzles. J Propul Power 13:444–445
8. Thies AT, Tam CKW (1996) Computation of turbulent axisymmetric and non-axisymmetric jet flows using the $k-\varepsilon$ model. AIAA J 34:309–316
9. Chenault CF, Beran P (1999) Numerical investigation of supersonic injection using a Reynolds-stress turbulence model. AIAA J 37:1257–1269
10. Zhang H, So R, Gatski T, Speziale C (1993) A near wall Second order closure for compressible turbulent flows, near-wall turbulent flows. Elsevier, New York, pp 209–218
11. Dembowski MA, Georgiadis NJ (2002) An evaluation of parameters influencing jet mixing using the WIND Navier–Stokes codes. NASA/TM-211727
12. Xiao Q, Tsai HM, Papamoschou D (2007) Numerical study of jet plume instability from an over-expanded nozzle, 45th AIAA aerospace sciences meeting and exhibit. AIAA, Nevada
13. Balabel A, Hegab AM, Wilson S, Nasr M, El-Behery S (2009) Numerical simulation of turbulent gas flow in a solid rocket motor nozzle. In: 13th International conference on aerospace science and aviation technology, Egypt
14. Balabel A, Hegab AM, Nasr M, El-Behery S (2011) Assessment of turbulence modeling for gas flow in two-dimensional convergent–divergent rocket nozzle. Appl Math Model 35:3408–3422
15. Fluent (2006) User's guide fluent 6.3.26. Fluent Incorporated, Lebanon
16. Ananthesha SN, Sridhara Vamsidhar D (2007) Numerical investigation and parametric study of fluidic thrust vectoring by shock vector control method. SASTech 5:58–65
17. Menter FR (1994) Two-equation eddy-viscosity turbulence models for engineering applications. AIAA J 32:1598–1605
18. Farokhi S (2014) Aircraft propulsion, 2nd edn. Wiley, New York
19. Krishnamurty VS, Shyy W (1997) Effect of wall roughness on the flow through converging-diverging nozzles. J Propul Power 13:753–762

View publication stats